Physical and numerical modeling of 1-D infiltration in sand-geotextile layers

Greg Siemens and Richard J. Bathurst
GeoEngineering Centre at Queen's-RMC, Royal Military College of Canada, Civil Engineering Department, Kingston, Ontario, Canada

ABSTRACT
Geotextiles are widely used for filtration and separation in earth structures. They are designed assuming saturated conditions based on their Apparent Opening Size or Filtration Opening Size and saturated hydraulic conductivity. However in the field, geotextiles may exist in an unsaturated state for much of their life. The transition from unsaturated to saturated states can lead to ponding of water due to a capillary break mechanism which may be detrimental to the hydraulic performance of the system. This paper describes experimental results and numerical simulations of unsaturated-saturated infiltration experiments on sand columns with a single geotextile layer inclusion. In the experiments, ponding pressure developed above the geotextile during infiltration. In order to match the measured ponding pressure and progression of the water front in the numerical simulations, the hydraulic properties of the geotextiles were adjusted to reduce hydraulic conductivity function values. A parametric study was carried out using adjusted hydraulic values and a wide range of geotextile thickness and saturated hydraulic values. A unique relationship between ponding head and permittivity of the geotextile was found for the boundary conditions and sand material used in the original physical column tests.

RÉSUMÉ
Les géotextiles sont largement utilisés pour la filtration et la séparation dans les ouvrages en terre. Ils sont conçus d'après leur Ouverture de Filtration en supposant des conditions hydrauliques saturées. Cependant, sur place, les géotextiles peuvent être en état non-saturé pour une bonne partie du temps. La transition de l'étal non-saturé à l'état saturé peut mener à l'accumulation d'eau causée par un mécanisme de coupure de capillarité qui peut nuire au rendement hydraulique du système. Cet article présente des résultats expérimentaux et des simulations numériques d'expériences d'infiltration en colonnes de sable non-saturé – saturé comportant une seule couche de géotextile. Dans ces expériences, une pression due à l'accumulation d'eau s'est développée au-dessus du géotextile durant l'infiltration. Dans le but de rapprocher la pression due à l'accumulation d'eau et la progression de l'eau dans les simulations numériques, les propriétés hydrauliques des géotextiles furent modifiées pour réduire leur conductivité hydraulique. Une étude paramétrique fut réalisée en utilisant des valeurs hydrauliques ajustées et une gamme étendue d'épaisseurs et de conductivités hydrauliques saturées des géotextiles. Une relation unique entre la charge hydraulique due à l'accumulation d'eau et la permittivité des géotextiles a été observée pour les conditions aux limites et les sables utilisés dans les essais en colonne physique originaux.

1 INTRODUCTION

Geotextiles are widely used for filtration and separation functions in earth structures. In these applications, geotextiles are selected based on their Apparent Opening Size (AOS) or Filtration Opening Size (FOS) and saturated hydraulic conductivity (Holtz et al. 1997; Koerner 2005; CFEM 2006). However, in the field the selected geotextile may exist in an unsaturated state for much of its life. Unsaturated hydraulic properties of geotextiles can be very different from their saturated properties. For example, due to their relatively large pore structure, geotextiles will desaturate at suctions as low as 0.1-0.2 kPa (10-20 mm above the water table). The result is a reduction in hydraulic conductivity of several orders of magnitude following desaturation. At these low suctions, the geotextile is essentially non-conductive. Clearly, large reductions in hydraulic conductivity may significantly impact the performance of a geotextile as a filter or separator and thus the transient saturated-unsaturated hydraulic properties of geotextiles warrant investigation.

In this paper, results from a series of 1-D drainage and infiltration experiments previously reported by the writers are briefly reviewed. A 2.05 m-tall column apparatus was used to perform the experiments using sand alone and sand with a single layer inclusion of geotextile. The sand and sand-geotextile columns were created in a saturated state by soil pluviation and then subjected to drainage from the bottom of the apparatus. After the columns had drained, surface water infiltration was initiated using a constant head of water at the top of the column. Infiltration test results showed a detectable delay in progression of the water front below the geotextile layer in columns with a geotextile inclusion compared to the control column with sand alone. Once the water front reached the geotextile, a capillary break developed and ponding pressure increased above the geotextile until breakthrough occurred. The ponding pressure required for breakthrough was greater than the water entry value of the geotextile in all cases and varied with the saturated hydraulic conductivity of the geotextile.

This paper describes the general approach and results of a set of numerical simulations that were carried out to predict the pore-water response and water front advance in the experimental column tests. In order to get a reasonable match the index hydraulic properties of the geotextiles measured in-isolation had to be modified. This

was attributed to the reduction in conductivity of the geotextiles due to soil particle penetration in the sand-geotextile column tests is not reproduced in conventional permittivity test for geotextiles.

The numerical simulation model with adjusted hydraulic parameters as the control data is used to carry out a numerical parametric study to quantify the influence of geotextile thickness, hydraulic conductivity and permittivity on 1-D ponding above a geotextile inclusion. The lessons learned in this study are of value for future investigation of the unsaturated-saturated hydraulic response of geotextile earth structures to surface water infiltration using numerical modelling.

2 PHYSICAL TESTS

2.1 Test Column and Methodology

The apparatus used to perform the sand and sand-geotextile infiltration tests is shown in Figure 1. The test methodology is reported in detail by Bathurst et al. (2007) and is only briefly described here. A control test with sand only and four tests with the same sand and a different single layer of geotextile were carried out. The sand was placed by pluviating through water. In the tests that included a geotextile, the geotextile was placed at a depth of 1200 mm from the surface. Following placement of the rest of the sand, the column was drained by opening a valve at the free water boundary shown in Figure 1. Equilibrium of the sand with the pore pressure environment was determined from tensiometer measurements which reached equilibration at an average suction of 1.1 kPa and then the valve was closed. Infiltration tests began by applying 100 mm constant head at the surface. The wetting front proceeded from the surface to the free water boundary. Progression of the water front was monitored using conductivity probes along the length of the column. Pore pressures were measured in the vicinity of the geotextile layer. When the water front reached the free water boundary it filled up the sand column and the full-height stand pipe so that at the end of the test a hydrostatic water pressure distribution was achieved.

2.2 Sand

The sand used in the physical tests is a synthetic olivine material classified as poorly graded sand (SP) according to the Unified Soil Classification System. Details of the physical properties of the sand are described in detail by Bathurst et al. (2007, 2009). The as-placed porosity was 0.52 and the hydraulic conductivity of the sand was measured as 2.0×10^{-3} m/s (Table 1).

The water retention values of the sand were measured using a Tempe cell. The measured wetting points are plotted in Figure 2 along with the Fredlund and Xing (1994) fitted curve for the wetting soil-water characteristic curve (SWCC). It should be noted that the $K_{sat(sand)}$ value used in the numerical modelling is well within measurement accuracy of the measured value. However, reducing the measured value by only 1% resulted in a detectable improvement in the match between physical and numerical results for water front advance in the column apparatus.

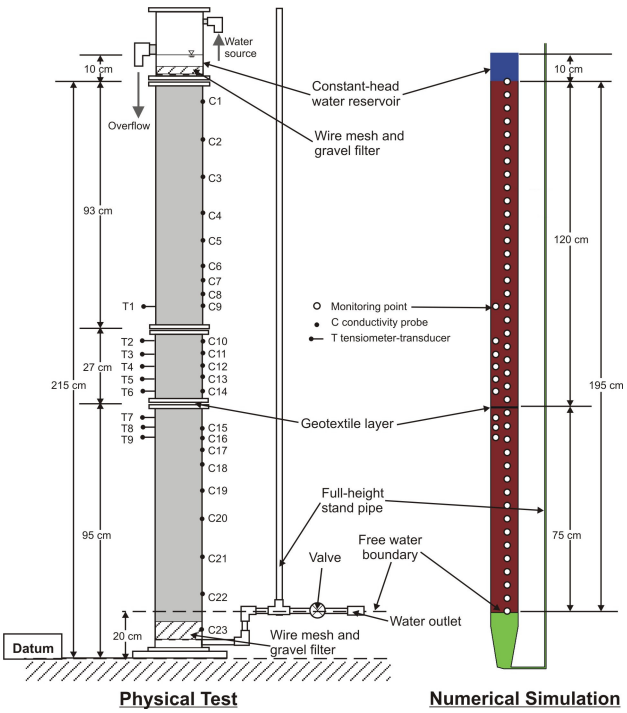

Figure 1. Schematics of the column test apparatus and numerical model geometry

Table 1. Index (measured) and adjusted (modelled) parameters for sand.

Parameter	Index value	Adjusted value
Porosity, (-)	0.52	0.52
Saturated hydraulic conductivity, $K_{sat(sand)}$ (m/s)	$2.0\text{x}10^{-3}$	$1.98\text{x}10^{-3}$

2.3 Geotextiles

Two typical commercially available geotextiles were used in the column tests. Properties of the geotextiles used in the numerical simulations are given in Table 2 and 3. Properties for the geotextiles were determined from in-isolation tests of compressibility, permittivity and water retention characteristics (pressure plate tests) (Bathurst et al. 2007, 2009).

One material was a woven geotextile manufactured from polypropylene slit film monofilament. The second geotextile was nonwoven manufactured from continuous entangled polypropylene filament. To broaden the range of hydraulic properties the geotextiles were modified by the addition of a kaolin paste. Infiltration tests were carried out on sand columns with new and modified geotextile inclusions to assess the impact of clogging on

infiltration behaviour and to create a wider range of geotextile-sand hydraulic response.

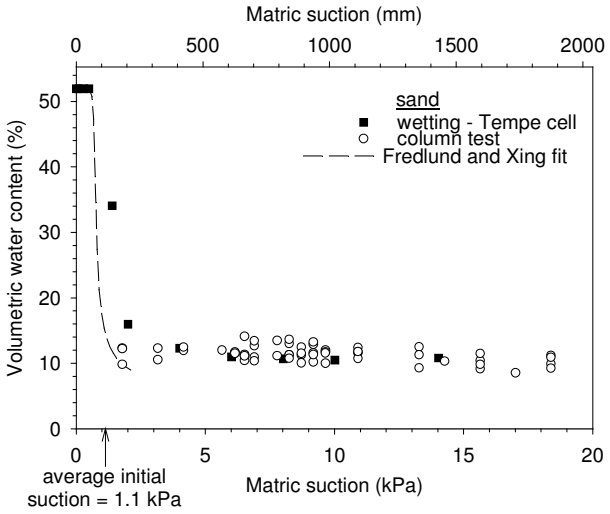

Figure 2. Wetting soil-water characteristic curve (SWCC) of sand

Table 2. Model parameters for new and modified woven geotextiles.

Parameter	New woven	Modified woven
Thickness, t_g (mm)	1.8	1.8
Porosity	0.72	0.64
Permittivity*, Ψ, (s^{-1})	0.0078	0.011
Saturated hydraulic conductivity*, $K_{sat(geotextile)}$ (m/s)	2.0×10^{-5}	1.4×10^{-5}

Note: * adjusted values

Table 3. Model parameters for new and modified nonwoven geotextiles.

Parameter	New nonwoven	Modified nonwoven
Thickness, t_g (mm)	3.8	3.8
Porosity	0.86	0.32
Permittivity*, Ψ, (s^{-1})	0.053	0.0024
Saturated hydraulic conductivity*, $K_{sat(geotextile)}$ (m/s)	2.0×10^{-4}	9.0×10^{-6}

Note: * adjusted values

For numerical simulations the relevant properties are the thickness, saturated hydraulic conductivity and geotextile-water characteristic curves (GWCCs).

Geotextiles compress under vertical pressure. In the column tests, the geotextile inclusions were placed at 1200 mm below the surface. From one-dimensional compression tests performed on the geotextile specimens this depth corresponded to a thickness (t_g) of 1.8 mm and 3.8 mm for the woven and nonwoven geotextiles, respectively. In practice, geotextile thickness cannot normally be measured to an accuracy of ±0.1 mm. According to ASTM D5199 (ASTM 2006), the measurement repeatability limit is ±14% for thickness of a geotextile under a 2 kPa load. This level of accuracy corresponds to ±0.25 mm and ±0.53 mm for the woven and nonwoven geotextiles, respectively. However, in the calibration and parametric analyses to follow, the numerical simulation results were found to be sensitive to small changes in geotextile thickness. Therefore, geotextile dimensions were defined to this level of accuracy.

The permittivity (Ψ) of the woven and nonwoven geotextile materials was measured in both new and modified conditions (Bathurst et al. 2009). The measured values were converted to hydraulic conductivity using

$$K_{sat} = \Psi \times t_g \qquad [1]$$

where: K_{sat} = saturated hydraulic conductivity in the direction normal to the plane of the geotextile (i.e. cross-plane direction). As expected, this equation shows that hydraulic conductivity decreases with decreasing thickness.

GWCCs for the woven and nonwoven geotextiles in new and modified conditions were measured using a Tempe cell (Bathurst et al. 2009). The measured data points during wetting are shown in Figure 3 together with Fredlund and Xing (1994) fits for the wetting curves. The corresponding unsaturated hydraulic conductivity curves are plotted in Figure 4. The Leong and Rahardjo (1997) fitting curves were used to model the unsaturated portion of the hydraulic conductivity curves. It should be noted that the transition range for the GWCC (suction range between the air entry value and the residual saturation) is extremely small. The transition occurs at approximately 0.05 kPa for the nonwoven new geotextile and at 0.6 kPa for the modified woven geotextile. The steepness of the GWCC data poses a challenge when attempting to fit curves to the data points. However, in the simulations that follow it was found that beyond a critical slope value there was no influence on column test results. Hence, a close fit to the measured data points in the transition zone was difficult to achieve but not necessary to achieve a good match between physical and numerical results.

Comparing the geotextile and sand unsaturated hydraulic conductivity curves (Figure 4) predicted using Leong and Rahardjo (1997) functions shows that the geotextile hydraulic conductivity values are lower than the sand over the selected range. The steep GWCC curves (Figure 3) are consistent with the steep curves in Figure 4. The hydraulic conductivity of the geotextiles drops several orders of magnitude in the vicinity of 0.1 kPa. This is consistent with the geotextiles being essentially hydraulically non-conductive at suctions greater than their water entry value (suction at residual saturation) as was reported by Bathurst et al. (2009).

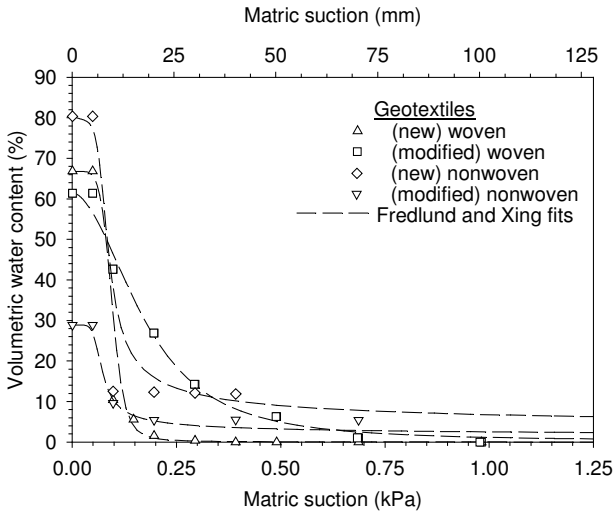

Figure 3. Wetting geotextile-water characteristic curves (GWCCs)

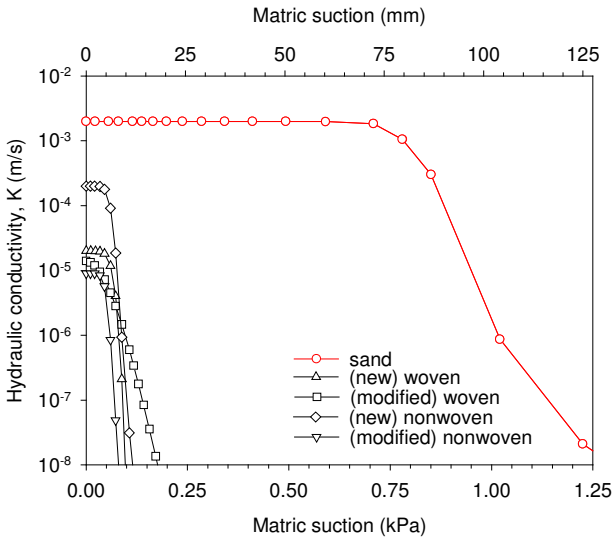

Figure 4. Unsaturated hydraulic conductivity versus matric suction using functions from Leong and Rahardjo (1997)

3 PHYSICAL TEST RESULTS

Results from the physical infiltration column tests are shown in Figure 5 and 6. Tensiometer measurements versus time for the sand modified-nonwoven geotextile column are plotted in Figure 5 and pore-water pressure profiles versus depth from the sand modified-woven geotextile column are shown in Figure 6.

The pore-water pressure recorded by instrument T1 in the sand modified-nonwoven geotextile test remained constant at about -1.1 kPa (– 110 mm) from t = 0 to 130 s, while the wetting front was above the instrument elevation (Figure 5). Thereafter, T1 registered a sharp increase in pore-water pressure before stabilizing at a reading of about 0 kPa. The change in pore-water pressure from negative to 0 kPa was consistent with the wetting front breaking the initial capillary suction in the sand column which led to a higher level of saturation. For the column test with sand only (data not plotted), the pore-water pressure reading for T1 remained at 0 kPa for the next 115 seconds (from t = 130 to 245 s). The pore-water pressure gradually increased as the wetting front advanced to the free water table at the bottom of the sand column. In the sand modified-geotextile column (Figure 5) a second jump in pore-water pressure occurred when the water front reached the geotextile layer at t = 160 s. The reason for the second jump in pore pressure is due to the geotextile having lower hydraulic conductivity than the sand. In order to maintain water front advance an increase in hydraulic gradient is required above the geotextile. In addition, a reduction in the water front progression was observed below the geotextile also due to a reduction in hydraulic conductivity.

When the wetting front reached the free water table at t = 310 s, the pore-water pressure at T1 increased rapidly. The onset of positive pore-water pressure generation can be understood to occur once there was a continuous hydraulic connection between saturated pore volumes along the entire column height. At about t = 550 s, the pore-water pressures were hydrostatic in the sand-geotextile column, and the hydrostatic pressure measured at tensiometer T1 reached the theoretical value of 9.4 kPa (960 mm). It should be noted that the nonlinear pore-water pressure response with time after the infiltration front reaches the free-water boundary is due in part to the venting of air and flow of water into the manometer lines at the base and sides of the column. A second mechanism may be local compression of entrapped air within the sand and geotextile. For the idealized case of no air present in the sand column and a perfect free boundary water condition, the pore-water response would instantaneously go to the maximum theoretical hydrostatic pressure value once the wetting front reached the free water boundary.

Pore-water response curves for devices T7 and T9 located 50 mm and 220 mm (respectively) below the geotextile layer are also plotted in Figure 5. During infiltration, the time for the wetting front to reach these instruments was longer due to their greater depth in the column. The period during which the pore-water pressure remained at 0 kPa decreased because the wetting front had less distance to travel to the free water boundary after passing the location of device T7. The final pore pressure measured by T7 was close to the theoretical hydrostatic pressure value of 13.2 kPa.

For the other tests with a geotextile layer, the response curves for T1 are qualitatively similar to the modified-nonwoven geotextile case shown in Figure 5. There were some differences in the magnitude of the second jump in pore-water pressure measured above the geotextile (Bathurst et al. 2009). Figure 6 shows that the water front progresses towards the geotextile unimpeded; however, as the water front crosses the geotextile a jump in pore pressure is recorded. While not shown here, the jump in the sand modified-woven geotextile case is less than for the column with the modified-nonwoven geotextile. The magnitude of the ponding was lowest for

the new nonwoven geotextile with the highest saturated conductivity and greatest for the modified nonwoven geotextile specimen with the lowest saturated conductivity. Once the columns were saturated the pore-water pressure response curves began to approach the response recorded for the control test and eventually terminated at the same theoretical hydrostatic pressure value. Similar pore-water pressure response was recorded for all tensiometer devices located above the geotextile in the sand-geotextile column tests prior to the wetting front reaching the geotextile.

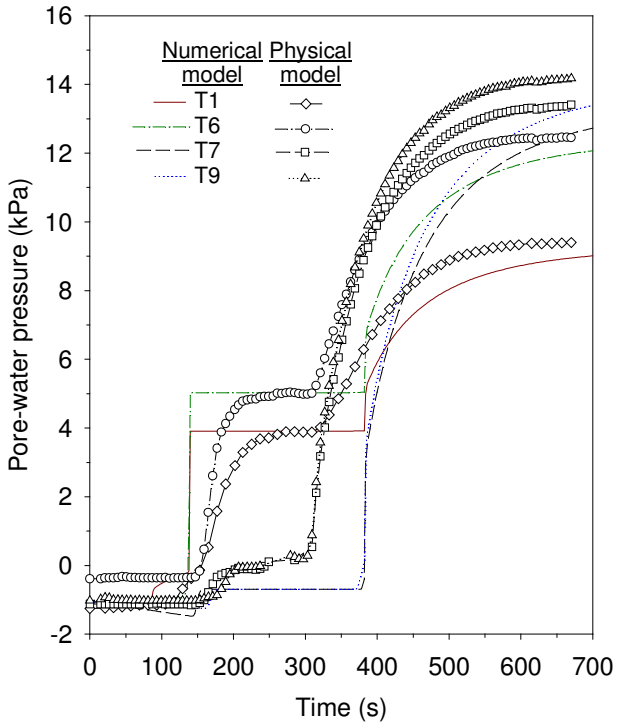

Figure 5. Measured and predicted pore-water pressures versus time for sand column with modified-nonwoven geotextile

4 NUMERICAL SIMULATIONS

The modelling approach was the same for all simulations in this investigation. Numerical calculations were performed using program SVFlux v5.10 (2004). The same model parameters were used for the sand above and below the geotextile. The model parameters for the GWCCs were applied to a thin region of the numerical domain with the same geotextile thickness and elevation as the physical tests (Figure 1). The objective of the first set of numerical models was to match the measured pore-water pressures recorded by tensiometers as well as the water front advance with infiltration time. This required adjustment of some of the independently determined geotextile parameters described earlier. The "calibrated" model values were used to generate the numerical simulation curves presented in Figure 5 and 6.

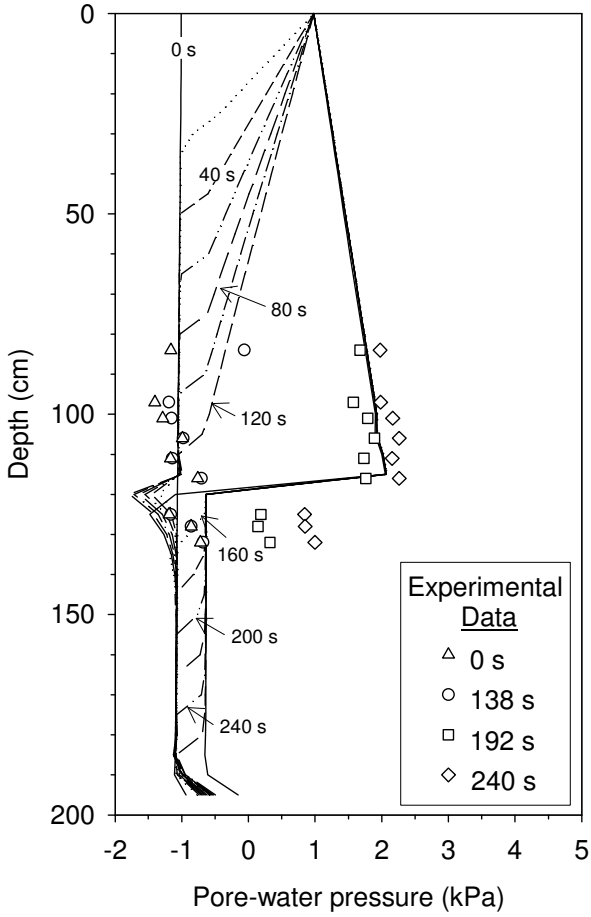

Figure 6. Pore-water pressure profiles at selected times for sand column with modified-woven geotextile

The reasons for and the magnitude of parameter adjustments are described here. The measured permittivity, thickness values and derived saturated hydraulic conductivity of the geotextiles were first used in the column test simulations. However, this resulted in negligible ponding and little change in the rate of water front advance below the geotextile as was observed in the physical testing. In order to predict the measured ponding pressures the saturated hydraulic conductivity was reduced by up to two orders of magnitude for each geotextile (the adjusted values are given in Table 2 and 3). The reason for the required reduction in conductivity is attributed to intrusion of sand particles into the geotextile following placement in the column. The permittivity tests were performed in-isolation without soil surrounding the geotextile and are therefore upper bound values. A similar corresponding reduction in geotextile saturated hydraulic conductivity has been reported in earlier simulation attempts of the RMC column tests by Ho (2000) and Iryo and Rowe (2004) to achieve a closer match with experimental results.

The control sand column required only a small modification to the hydraulic conductivity value to match

the measured rate of infiltration front advancement as noted earlier.

Results for the calibrated models are shown in Figure 5 and 6. In the sand modified-nonwoven geotextile column, the predicted pore pressures are consistent with measured values from 0-80 s. When the water front passes the T1 monitoring point, the pore pressure jumps and approaches 0 kPa. When the water front reaches the modified nonwoven geotextile a second jump in pore pressure is recorded since an elevated ponding pressure is required to push the water through the geotextile. In the numerical simulation the jump occurs over less than one second compared with 40-50 s in the physical tests. This is due to compression of the air phase within the soil in the physical experiments as well as possible small delays in response time of the tensiometer devices (Bathurst et al. 2007). Similar jumps are noted at the monitoring points below the geotextile; thereafter, pore pressure remains constant until the water front reaches the free water boundary. At this point the stand pipe fills up and the pore pressure regime approaches hydrostatic conditions.

The numerical simulations allow the entire pore-water response history of the columns to be tracked for the duration of the test. The numerical results for the sand modified-woven geotextile column test simulation are plotted in Figure 6. Initially the entire column is at -1.1 kPa pressure. At locations where tensiometer readings were taken, there is judged to be reasonably good agreement between predicted and measured values as the water front progresses downward. When the water front reaches the geotextile the water mounds to a pressure head greater than the applied 100 mm head at the surface in order to push the water through the 'bottleneck' provided by the geotextile. Finally the water front continues towards the free water boundary. However, the rate of advance is less than that for the water above the geotextile (e.g. compare vertical distance between 40 s increment pore-water isochrones).

5 PARAMETRIC ANALYSES

Following model calibration using the sand and sand-geotextile tests, three sets of numerical parametric analysis were undertaken to examine the influence of geotextile properties on column response. The first parametric analysis included varying the GWCC. However, the shape of the GWCC was found to have little effect on the maximum ponding pressure and progression of the water front. Hence, these results are not presented here. The second parametric analysis examined the influence of hydraulic conductivity of the geotextile on column response. In the third set of analyses the geotextile permittivity was varied by changing the thickness and hydraulic conductivity of the material (see equation [1]).

As noted in the previous model calibration section, the influence of the magnitude of saturated hydraulic conductivity of the geotextile on numerical results is significant. To expand the database of numerical simulations using the reference column tests, the saturated hydraulic conductivity of the four geotextiles was varied from 4×10^{-3} m/s to 9×10^{-6} m/s (e.g. $K_{sat(sand)}$ / $K_{sat(geotextile)}$ varied from 2 to 220).

Results are presented in Figure 7 using ratios of the adjusted saturated hydraulic conductivity of the sand and geotextile as the independent parameter. The data show that ponding pressure (or head) increases nonlinearly with decreasing geotextile conductivity (increasing $K_{sat(sand)}$ / $K_{sat(geotextile)}$). Second order polynomial curves plotted with the data show good visual agreement with numerical results. Interestingly, the results of new and modified geotextiles using calibrated hydraulic parameters plot together on the two curves representing geotextile layers with different thickness. It appears that the thickness of the geotextile is an important factor that influences ponding pressures when all other parameters are held constant.

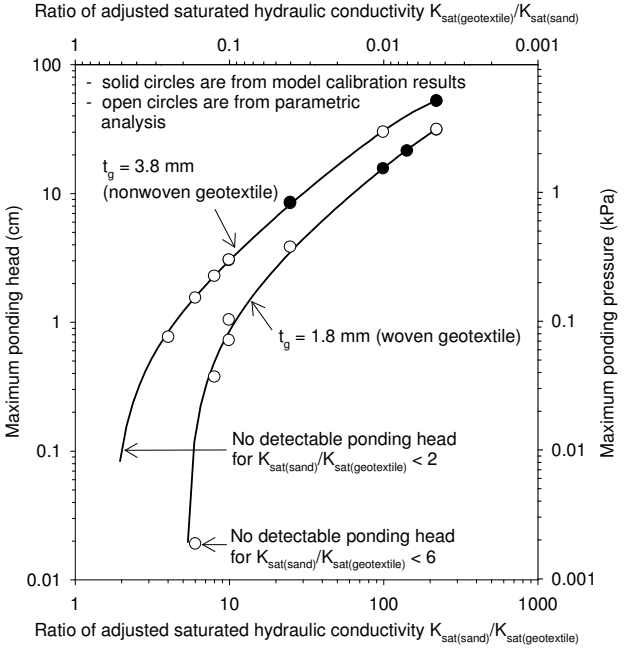

Figure 7. Influence of geotextile thickness and saturated hydraulic conductivity on maximum ponding head.

The plots also show that below a threshold value of $K_{sat(sand)}$ / $K_{sat(geotextile)}$ ponding heads are negligible. This value is taken as $K_{sat(sand)}$ / $K_{sat(geotextile)}$ = 2 for the models with 3.8 mm thick geotextiles and $K_{sat(sand)}$ / $K_{sat(geotextile)}$ = 6 for the 1.8 mm thick geotextiles. At first, this result appears to conflict with the recommendation by Bathurst et al. (2009) to limit $K_{sat(sand)}$ / $K_{sat(geotextile)}$ to not more than 0.1 in order to prevent ponding. However, this recommendation was based on hydraulic conductivity ratios computed using the index values for the geotextiles. Recall that these values must be reduced by up to two orders of magnitude to match the physical column test results (adjusted values are shown in Table 2 and 3). Recall also the strong influence of the geotextile thickness on the numerical simulations and the practical limitations of measuring this parameter. Therefore, the earlier recommendation by the writers is still valid since

designers will have available only measured in-isolation hydraulic conductivity values. What this paper demonstrates is that in order to extend the database of physical tests first reported by Bathurst et al. (2009) using numerical simulations, the saturated hydraulic conductivities of the geotextiles determined from conventional laboratory tests must be reduced.

The data in Figure 7 show that hydraulic conductivity and thickness of the geotextile both influence column response. Therefore the influence of permittivity on hydraulic response of numerical columns was investigated. The thickness of the new and modified geotextiles was varied over the range 0.8 to 9.8 mm while keeping the GWCC and saturated hydraulic conductivity constant for each geotextile. This range of thickness captures a large number of potential geotextile materials. The numerical results are plotted **Error! Reference source not found.**as maximum ponding head (or pressure) versus adjusted permittivity using log-linear axes. In general, as permittivity deceases, maximum ponding head increases. Above a permittivity value of approximately Ψ = 0.13 s^{-1}, no ponding is observed. Based on visual observation, two breakpoints in the data are selected at permittivities of 0.06 s^{-1} and 0.0115 s^{-1} and thus a tri-linear approximation can be fitted to the data.

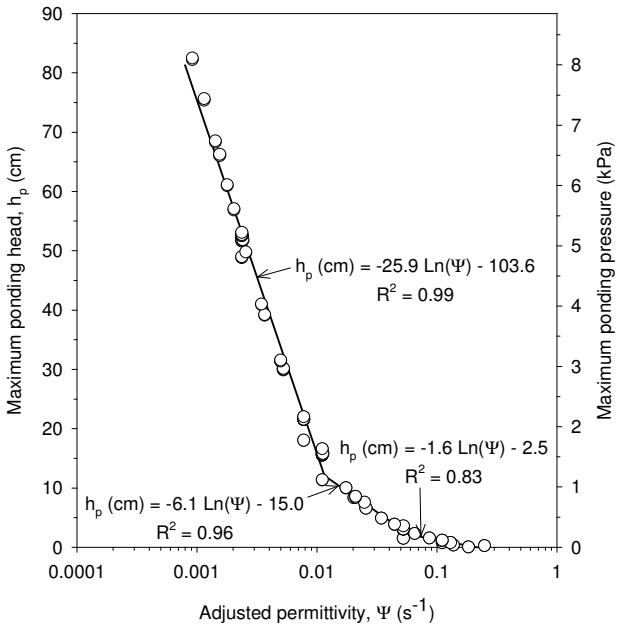

Figure 8. Maximum ponding head versus adjusted geotextile permittivity

The data in Figure 8 may be useful for the design of sand-geotextile systems subject to surface water infiltration loading when potential water ponding leading to horizontal migration of the water along the geotextile surface is undesirable (e.g. in reinforced soil walls). However, this data was determined using adjusted values from numerical simulations. A design methodology should use the procedures described in this paper: scaling index values of geotextile hydraulic conductivity, estimating the insitu (compressed) geotextile thickness and using Figure 7 or 8 to assess the maximum ponding head under surface infiltration conditions.

Nevertheless, the quantitative conclusions made with respect to Figures 7 and 8 in this paper are likely valid only for the soil type, boundary conditions and configuration used in the physical and numerical models. Other soils with different particle size distributions, porosity and hydraulic conductivity can be expected to generate a different hydraulic response and hence a different ponding head-permittivity relationship. Therefore, different recommendations regarding a critical permittivity value will apply for other soil materials for design.

6 CONCLUSIONS

This paper presents results of selected physical tests and numerical simulations of 1-D infiltration tests on unsaturated sand and sand-geotextile columns. Input parameters used in numerical simulations were adjusted to improve the match between measured hydraulic response in physical column tests and predicted response. Numerical simulation results were consistent with physical test results by showing that a geotextile can cause a detectable delay in the progression of the water front below the geotextile and generate a sustained ponding head above the geotextile. The calibrated model is used to carry out a parametric analysis to investigate the influence of geotextile permittivity on potential water ponding over a geotextile layer in sand. For the range of geotextile parameters investigated in combination with a single sand type, the parametric study identified a minimum adjusted permittivity value above which ponding heights are negligible as well as a unique relationship between adjusted permittivity and maximum ponding head. Finally, quantitative results and conclusions must be restricted to the range of parameter values investigated in this study.

ACKNOWLEDGEMENTS

The work described in this paper was supported by grants awarded to the authors by the Natural Sciences and Engineering Research Council of Canada, the Academic Research Program at RMC, the Department of National Defence (Canada) and British Petroleum (formerly Amoco).

REFERENCES

ASTM 2006. Standard Test Method for Measuring the Nominal Thickness of Geosynthetics. ASTM standard D5199. American Society for Testing and Materials International (ASTM) West Conshohocken, PA.

Bathurst, R.J., Ho, A.F. and Siemens, G.A. 2007. A column apparatus for investigation of 1-D unsaturated-saturated response of sand-geotextile systems. ASTM Geotechnical Testing Journal 30(6): 433-441.

Bathurst, R.J., Siemens, G.A. and Ho, A.F. 2009. Experimental investigation of infiltration ponding in one-dimensional sand-geotextile columns. Geosynthetics International 16(3): 158-172.

Canadian Foundation Engineering Manual, 2006. Fourth Edition Canadian Geotechnical Society, Richmond, B.C, Canada, 488 p.

Fredlund, D.G. and Xing, A. 1994. Equations for the soil-water characteristics curve. Canadian Geotechnical Journal 31(4): 521-532.

Holtz, R.D., Christopher, B.R. and Ryan, R.B. 1997. Geosynthetic Engineering, BiTech Publishers, Richmond, British Columbia, Canada.

Koerner, R.M. 2005. Designing with Geosynthetics, Fifth Edition, Prentice Hall, Upper Saddle River, New Jersey, USA.

Leong, E.C. and Rahardjo, H. 1997. Permeability functions for unsaturated soils. Journal of Geotechnical and Geoenvironmental Engineering 123(12): 1118-1126.

Ho, A.F. 2000. Experimental and numerical investigation of infiltration ponding in one-dimensional sand–geotextile columns. MSc thesis, Queen's University, Kingston, Ontario, 212 p.

Iryo, T. and Rowe, R.K. 2004. Numerical study of infiltration into a soil–geotextile column. Geosynthetics International 11(5): 377–389.

SVFlux v5.10. SoilVision Systems Ltd., Saskatoon, Canada.